Ligand-Field Analysis of an Er(III) Complex with a Heptadentate Tripodal N_4O_3 Ligand

Bernadine M. Flanagan,[†] Paul V. Bernhardt,[†] Elmars R. Krausz,[‡] Stefan R. Lüthi,[†] and Mark J. Riley*,[†]

Department of Chemistry, University of Queensland, St. Lucia, 4072, Australia, and
Research School of Chemistry, Australian National University, Canberra, 0200, Australia

Received March 23, 2001

Polarized absorption and emission spectra of trigonal single crystals of an Er(III) complex coordinated to a heptadentate tripodal ligand are reported at temperatures between 8 and 298 K. The assigned energy levels below the onset of ligand absorption (<25 000 cm^{-1}) are fitted to a parametrized electronic Hamiltonian. The C_3 site symmetry of the Er(III) ion requires eight parameters for a full description of the ligand field within a one-electron operator description. This compound shows unusually large splittings of the multiplets, and the fitted parameters imply that this heptadentate ligand imparts the largest ligand field reported for an Er(III) complex. The ligand field was also interpreted within the angular overlap model (AOM). We derive the AOM matrix to include both σ and anisotropic π bonding and show that a useful description of the C_3 ligand field can be made using only five parameters. The success of the AOM description is encouraging for applications on isomorphous complexes within the lanthanide series and in describing the ligand field of low-symmetry complexes with less parameters than in the usual spherical harmonic expansion.

Introduction

There is considerable interest in lanthanide ions that are complexed with organic polydentate ligands. There is the possibility of sensitizing the lanthanide luminescence through energy transfer from the ligand, which may have a large absorption cross section.[1] The effectiveness of sensitization in solution depends on the extent to which the ligand shields the metal ion from interaction with solvent molecules. Solvent molecules can promote to nonradiative decay from the emitting level. This shielding is also relevant to the design of lanthanide-based contrast agents for magnetic resonance imaging.[2] In addition, a number of such polydentate erbium(III) complexes have recently been found to show electroluminescence in organic-based light-emitting diodes.[3,4]

Recently, we have demonstrated a new synthetic route to a series of isomorphous Ln(III) complexes with the heptadentate ligand trensal (H_3trensal = 2,2′,2″-tris-(salicylideneimino)-triethylamine).[5] Importantly, all the members of this series place the lanthanide ion on a C_3 crystallographic site, preserving the inherent symmetry of the complex. While these complexes are of relatively low symmetry, they still have the spectroscopic advantage of being in a uniaxial space group. In this study, we use low-temperature polarized absorption spectroscopy to assign 52 of the possible 53 energy levels lying below the onset of ligand absorption. The assignment is aided by low-temperature emission spectra. Luminescence is unusual in an Er(III) complex with organic ligands, as there are many high-energy vibrations that efficiently bridge the relatively dense f-electron ligand-field states with radiationless relaxation pathways. In fact, we will show that the ring vibrations are particularly effective at coupling to the electronic states. The vibronic transitions on a particular electronic state are shown to be enhanced when they are in resonance with the levels of a higher electronic state.

Experimental Section

Synthesis. Needle-shaped Er(trensal) single crystals were obtained[5] with typical dimensions of 100 × 100 × 300 μm. The Er(III) ion lies on a C_3 site of the $P\bar{3}c1$ space group of the Er(trensal) complex as shown in Figure 1. Details of the synthesis and structural characterization of this compound have been described previously.[5−7] The observation of the single crystals under a microscope with crossed polarizers reveals extinction directions parallel and perpendicular to the needle axis, which was identified as the crystallographic **c** axis.

Instrumentation. Absorption spectra were recorded at 295 and 10 K on a single-beam absorption instrument.[7] The light of a 150 W halogen lamp was dispersed with a Spex 1701 single monochromator, equipped with a 1200 lines/mm grating blazed at 500 nm (for spectra in the range of 375−825 nm) or a 600 lines/mm grating blazed at 1.6 μm (775−2500 nm). The light was focused on the masked sample using cassagrain optics, and the transmitted light was detected with either an S-20 photomultiplier tube (375−825 nm) or a liquid N_2-cooled InSb diode (775−2500 nm). Overview and high-resolution scans of the compound were made with a typical resolution of 2 cm^{-1} at 295 and 10 K for σ and π polarization (the electric vector of the electromagnetic field being perpendicular and parallel to the crystal **c** axis, respectively) as well as for randomly polarized light. The sample absorbance was calculated from the transmitted intensities of the single-beam spectra with and without the sample.

The luminescence spectra of powdered samples of Er(trensal) were measured using the 356.4 and 350.7 nm lines of an Kr^+ ion laser (Spectra Physics model 165). The sample luminescence was dispersed with a Spex 1401 double monochromator, equipped with 1200 lines/

* To whom correspondence should be addressed.
[†] University of Queensland.
[‡] Australian National University.

(1) Balzani, V.; Scandola, F. *Supramolecular Photochemistry*; Horwood: Chichester, 1991.
(2) Lauffer, R. B. *Chem. Rev.* **1987**, *87*, 901.
(3) Curry, R. J.; Gillin, W. P. *App. Phys. Lett.* **1999**, *75*, 1380.
(4) Sun, R. G.; Wang, Y. Z.; Zheng, Q. B.; Zhang, H. J.; Epstein, A. J. *J. Appl. Phys.* **2000**, *87*, 7589.
(5) Bernhardt, P. V.; Flanagan, M. B.; Riley, M. J. *Aust. J. Chem.* **2000**, *53*, 229.
(6) Kanesato, M.; Yokoyama, T. *Chem. Lett.* **1999**, 137.
(7) Kanesato, M.; Yokoyama, T.; Itabashi, O.; Suzuki, T. M.; Shiro, M. *Bull. Chem. Soc. Jpn.* **1996**, *69*, 1297.

10.1021/ic0103244 CCC: $20.00
Published on Web 09/06/2001

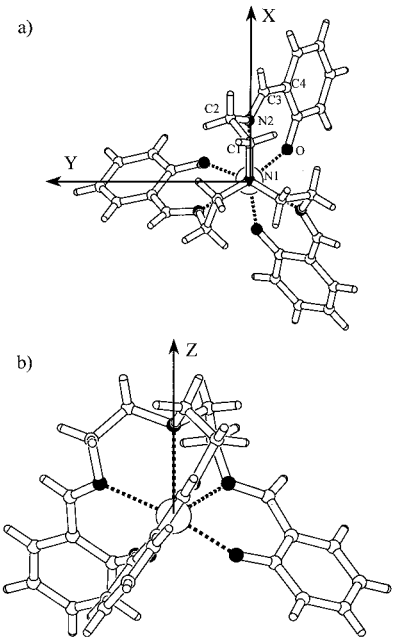

Figure 1. Molecular structure of Er(trensal): (a) viewed along the **c** axis showing the labels of the atoms, coordinating atoms are shown in black; (b) approximately edge-on to the N2−Er−O bidentate ring showing the angle that this makes with the trigonal axis.

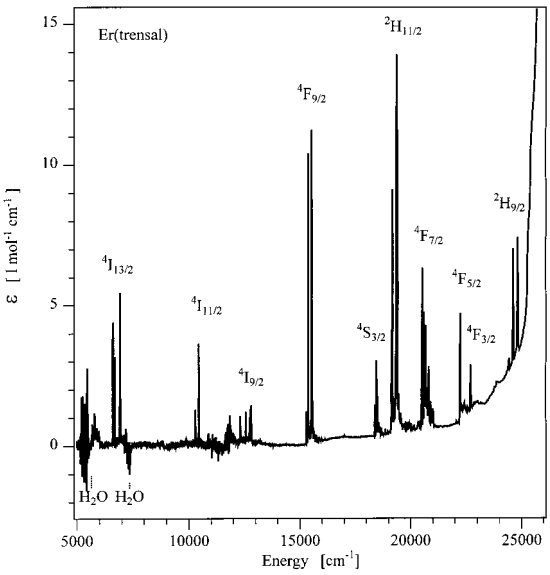

Figure 2. Unpolarized overview absorption spectrum of Er(trensal) recorded at a temperature of 10 K. The Er(III) SLJ multiplets are indicated. At 25 000 cm^{-1} the onset of the ligand absorption occurs. Overtone vibrations of H_2O are visible at 5000 and 7500 cm^{-1}. The bad signal-to-noise ratio around 12 000 cm^{-1} is due to lack of sensitivity of the detectors (S-20 PMT and InSb diode) in this spectral range.

mm gratings blazed at 500 nm, and detected with a photomultiplier tube (RCA 31034A) in photon-counting mode. The signal was passed through a preamplifier (Stanford SR445) and acquired with a photon-counting system (Stanford SR400). The luminescence spectra were corrected for the response of the detection system using a calibrated tungsten band lamp with a color temperature of 2590 K.[8] The spectra were transformed into units of photon flux (cm^{-1} s) vs wavenumber (cm^{-1}).[9] For absorption and luminescence experiments at 10 K, the samples were cooled in a helium flow-tube cryostat.

Results

Absorption Spectra. An overview of the absorption spectrum of Er(trensal) is shown in Figure 2. The overall energies and intensities of these 4f−4f excitations are typical for Er(III) compounds. A closer inspection, however, reveals a number of peculiarities. First, it appears that the trensal ligand provides a relatively strong ligand-field environment for the Er(III) ion. This results in both the higher baricenter energies of the SLJ multiplets as well as the larger overall ligand-field splittings within these SLJ multiplets. Compared with those of the trigonal $Er(ODA)_3^{3-}$ complex (ODA = oxydiacetate), for example, the multiplet splittings are ∼50−100% larger in the present compound.[10] The observed transition energies for Er(trensal) are given in Table 1. Second, some transitions (particularly the $^4I_{15/2} \rightarrow {}^4F_{7/2}$ transition) show lines in addition to the electronic origins which are due to vibronic transitions. This is unusual as it is expected that the symmetry-allowed electronic transitions would be much more intense than the vibronic ones.

Luminescent Transitions. The 4f−4f luminescence is not a common phenomenon for Er(III) that is coordinated with organic ligands. This is due to the high-vibrational energies of the organic ligands. Nonradiative relaxation is proportional to the energy of the highest energy vibrations present in the compound.[11,12] Spectroscopic studies on various rare-earth-doped compounds lead to the following rule of thumb: energy gaps between neighboring 4f states, corresponding to less than 6 quanta of the highest energy vibration present in the compound, occur nonradiatively via multiphonon relaxation. Emission, however, will be a competing relaxation mechanism, if more than ∼6 quanta are required.[13,14] Typical vibrational energies of organic ligands are comparable to the largest splitting between neighboring 4f SLJ multiplets in Er(III), i.e., ∼3000 cm^{-1} (see Figure 2). The $^4S_{3/2} \rightarrow {}^4I_{15/2}$ luminescence in the title compound, at temperatures of 77 K and below, is therefore a remarkable observation (Figure 3). With an energy difference of 2833 cm^{-1}, the $^4S_{3/2}(1)-{}^4F_{9/2}(5)$ gap is the second largest energy difference between SLJ multiplets in this compound, followed by 2496 cm^{-1} for the $^4F_{9/2}(1)-{}^4I_{9/2}(5)$ gap. No emission could be observed from the $^4F_{9/2}$ multiplet at temperatures as low as 7 K. The largest energy gap is 5952 cm^{-1}, between the first excited- and the ground-state multiplets ($^4I_{13/2}(1)-{}^4I_{15/2}(8)$). No experiments were undertaken in this work to study this transition.

Ligand-Field Calculations. In C_3 symmetry the energy levels of the Er(trensal) complex are split into the 182 Kramers doublets of the f^{11} configuration, of which 53 fall into the transparent region of the crystal. Of these 53 possible transitions we observe all but one. Their assignments can be made on the basis of the polarization properties of their spectra. For electric dipole allowed transitions, the selection rules are the same as those for the other trigonal groups D_3 and C_{3v}. The Kramers doublets transform either as the Γ_4 and Γ_5 pair (hereafter abbreviated as $\Gamma_{4,5}$) or as the Γ_6 and Γ_6 ($\bar{\Gamma}_6$) pair of irreducible representations using the Bethe Γ notation.[15] In the Er(trensal)

(8) Krausz, E. R. *Aust. J. Chem.* **1993**, *46*, 1041.
(9) Ejder, E. *J. Opt. Soc. Am.* **1969**, *59*, 223.
(10) Schone, K. A.; Quagliano, J. R.; Richardson, F. S. *Inorg. Chem.* **1991**, *30*, 3803.
(11) Riseberg, L. A.; Moos, H. W. *Phys. Rev.* **1968**, *174*, 429.
(12) Dijk, J. M. F. v.; Schuurmans, M. F. H. *J. Chem. Phys.* **1983**, *78*, 5317.
(13) Hehlen, M. P.; Krämer, K.; Güdel, H. U.; McFarlane, R. A.; Schwartz, R. N. *Phys. Rev. B* **1994**, *49*, 12475.
(14) Riedener, T.; Güdel, H. U.; Valley, G. C.; McFarlane, R. A. *J. Lumin.* **1995**, *63*, 327.

Table 1. Experimental Energy Levels and Transition Line Strengths for Er(trensal)

		energy (cm^{-1})		obsd intens (10^{-42} esu^2 cm^2)				energy (cm^{-1})		obsd intens (10^{-42} esu^2 cm^2)	
multiplet	irrep[a]	obsd	calc	S_σ [D^2]	S_π [D^2]	multiplet	irrep[a]	obsd	calc	S_σ [D^2]	S_π [D^2]
$^4I_{15/2}$	$\Gamma_{4,5}$	0	0	0.005[b]		$^4F_{9/2}$	Γ_6	15 302	15 307	15.8	1.4
	$\Gamma_{4,5}$	54	54	0.235			$\Gamma_{4,5}$	15 328	15 317	16.4	4.2
	Γ_6	102	102	0.176			$\Gamma_{4,5}$	15 382	15 395	63.0	6.8
	$\Gamma_{4,5}$	110	110	0.202			Γ_6	15 538	15 552	100.2	7.2
	Γ_6	299	299	0.033			$\Gamma_{4,5}$	15 562	15 569	14.5	21.1
	$\Gamma_{4,5}$	568	567	1.000		$^4S_{3/2}$	$\Gamma_{4,5}$	18 395	18 420	1.3	3.8
	Γ_6	610	612	0.753			Γ_6	18 469	18 484	92.0	5.9
	$\Gamma_{4,5}$	642	641	0.229		$^2H_{11/2}$	$\Gamma_{4,5}$	19 157	19 186	34.3	12.1
$^4I_{13/2}$	$\Gamma_{4,5}$	6594	6590	21.9	14.9		Γ_6	19 165	19 194	87.0	7.2
	Γ_6	6611.5	6613	10.4	1.8		$\Gamma_{4,5}$	19 193	19 200	83.6	29.9
	$\Gamma_{4,5}$	6620.5	6630	34.1	31.4		$\Gamma_{4,5}$	19 371	19 359	143.5	32.7
	$\Gamma_{4,5}$	6690	6706	32.8	11.5		Γ_6	19 379	19 386	121.0	8.3
	$\Gamma_{4,5}$	6909	6937	19.0	0.0		$\Gamma_{4,5}$	19 412	19 404	56.2	20.1
	Γ_6	6928	6949	132.7	10.6	$^4F_{7/2}$	$\Gamma_{4,5}$	20 530	20 516	4.6	20.1
	$\Gamma_{4,5}$	6939	6967	12.2	0.0		$\Gamma_{4,5}$	20 613	20 615	2.5	25.3
$^4I_{11/2}$	$\Gamma_{4,5}$	10 290.5	10 270	17.2	2.1		Γ_6	20 679	20 665	6.5	1.9
	Γ_6	10 300.5	10 279	1.1	0.0		$\Gamma_{4,5}$	20 738	20 741	1.7	4.9
	$\Gamma_{4,5}$	10 315.5	10 302	2.5	0.0	$^4F_{5/2}$	$\Gamma_{4,5}$	22 244	22 234	3.7	13.6
	$\Gamma_{4,5}$	10 444	10 449	0.0	14.6		Γ_6	22 261	22 240	4.2	2.5
	Γ_6	10 448.5	10 459	27.5	14.8		$\Gamma_{4,5}$	22 353	22 326	1.6	11.9
	$\Gamma_{4,5}$	10 509.5	10 466	0.0	0.0	$^4F_{3/2}$	$\Gamma_{4,5}$	22 607	22 604	0.8	7.2
$^4I_{9/2}$	$\Gamma_{4,5}$	12 321	12 283	4.8	1.7		Γ_6	22 734	22 736	3.1	1.6
	Γ_6	12 532	12 531	1.5	0.0	$^2H_{9/2}$	$\Gamma_{4,5}$	24 434	24 424	16.5	2.2
	$\Gamma_{4,5}$		12 589	7.2	0.10		Γ_6	24 619	24 645	10.0	1.2
	Γ_6	12 768	12 728	21.5	2.4		$\Gamma_{4,5}$	24 628	24 672	5.0	3.9
	$\Gamma_{4,5}$	12 806	12 774	11.3	2.0		$\Gamma_{4,5}$	24 798	24 782	2.7	2.8
							Γ_6	24 841	24 836	11.7	2.9

[a] The $\Gamma_{4,5}$ and Γ_6 refer to the (Γ_4, Γ_5) and (Γ_6, Γ_6) Kramers doublets of the C_3 double group.[15] [b] Intensities given for the $^4I_{15/2}$ multiplet are the relative intensities of the unpolarized $^4I_{15/2} \leftarrow {}^4S_{3/2}$ luminescent transitions.

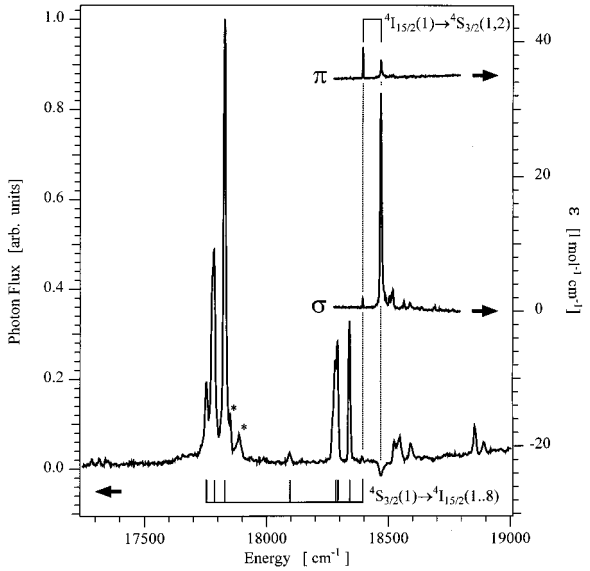

Figure 3. Detail of the $^4I_{15/2} \leftrightarrow {}^4S_{3/2}$ spectral region. All spectra are recorded at 10 K. The absorption spectra are shown in σ and π polarization with a spectral resolution of 0.06 nm. The luminescence spectrum was recorded at random polarization on a powder sample with a spectral resolution of 0.2 nm. The energy-level structure of the $^4I_{15/2}$ ground-state multiplet, assigned from the luminescence spectrum (bottom), as well as the experimentally assigned ligand-field levels of the $^4S_{3/2}$ states (top) are shown. The dotted lines indicate the electronic origins in both the absorption and luminescence spectra. The asterisks indicate unidentified artifacts.

complex, the ground state is a $\Gamma_{4,5}$ Kramers doublet and transitions will be electric dipole allowed to other $\Gamma_{4,5}$ states in both σ and π polarization. $\Gamma_{4,5} \leftrightarrow \Gamma_6$ transitions are electric dipole allowed in σ polarization only while $\Gamma_6 \leftrightarrow \Gamma_6$ transitions are electric dipole allowed in π polarization only. The low-temperature absorption spectrum will then contain spectral features that are weak or absent in π polarization, identifying them as transitions to a Γ_6 upper state. A low-temperature absorption spectrum is critical in making the assignments, as there are three components of the $^4I_{15/2}$ multiplet that are within ~110 cm^{-1} of the ground state. These low-lying states cause spectral congestion as they are populated at higher temperature.

Once the spectra are assigned, levels of the correct symmetry are calculated using a conventional electronic Hamiltonian, for f-electron systems, that includes both atomic and ligand-field parameters. The main atomic parameters are an average energy or offset term, E_{av}, the electron repulsion parameters, F^k (k = 2, 4, 6), and a spin−orbit coupling constant, ζ_{so}. It was found that the "minor" atomic parameters[16] α, β, γ, T^i (i = 2, 3, 4, 6, 7, 8), P^k (k = 2, 4, 6), and M^j (j = 0, 2, 4) have little influence on the fit over the range of levels being studied. A number of different sets of these minor parameters result in near identical fits. When allowed to vary, these parameters wander significantly from generally accepted values. This behavior is because the calculation is fitted to the observable transitions, which represent only the lowest one-third of the possible 182 energy levels. To circumvent this, in this work the 15 minor parameters were all fixed at the values found for $Er(ODA)_3^{3-}$ [10] although other sets, for example, that were found for Er(III):$LaCl_3$ worked equally as well.[17] The only exception was the parameter α where a slightly reduced value of 17.5 cm^{-1} was used. The ligand field was expanded in terms of the one-electron spherical tensor operator C_{kq}, which

(15) Koster, G. F.; Dimmock, J. O.; Wheeler, R. G.; Statz, H. *Properties of the Thirty-Two Point Groups*; MIT Press: Cambridge, 1963.

(16) Morrison, C. A.; Leavitt, R. P. In *Handbook on the Physics and Chemistry of the Rare Earths*; Gschneidner, K. A., Eyring, L., Eds.; North-Holland: New York, 1982; Vol. 5, pp 461−701.

(17) Huefner, S. *Optical Spectra of Transparent Rare Earth Compounds*; Academic Press: New York, 1978.

Table 2. The $D^{f}(\theta, \phi, \psi)$ Matrix

metal	σ	π_x	π_y
$\|\sigma>$	$\frac{1}{2}(5\cos^2\theta - 3)\cos\theta$	$\frac{1}{4}\sqrt{\frac{3}{2}}(5\cos 2\theta + 3)\sin\theta\cos\psi$	$\frac{1}{4}\sqrt{\frac{3}{2}}(5\cos 2\theta + 3)\sin\theta\sin\psi$
$\|\pi s>$	$\frac{1}{4}\sqrt{\frac{3}{2}}(5\cos 2\theta + 3)\sin\theta\sin\phi$	$\frac{1}{4}[(5\cos^2\theta - 1)(\cos\theta\sin\phi\cos\psi + \cos\phi\sin\psi) - 10\sin^2\theta\cos\theta\sin\phi\cos\psi]$	$\frac{1}{4}[(5\cos^2\theta - 1)(-\cos\theta\sin\phi\sin\psi + \cos\phi\cos\psi) + 10\sin^2\theta\cos\theta\sin\phi\sin\psi]$
$\|\pi c>$	$\frac{1}{4}\sqrt{\frac{3}{2}}(5\cos 2\theta + 3)\sin\theta\cos\phi$	$\frac{1}{4}[(5\cos^2\theta - 1)(\cos\theta\cos\phi\cos\psi - \sin\phi\sin\psi) - 10\sin^2\theta\cos\theta\cos\phi\cos\psi]$	$\frac{1}{4}[(5\cos^2\theta - 1)(-\cos\theta\cos\phi\sin\psi - \sin\phi\cos\psi) + 10\sin^2\theta\cos\theta\cos\phi\sin\psi]$
$\|\delta s>$	$\frac{\sqrt{15}}{2}\cos\theta\sin^2\theta\sin 2\phi$	$\sqrt{\frac{5}{8}}[\sin 2\theta(\cos\theta\sin 2\phi\cos\psi + \cos 2\phi\sin\psi) - \sin^3\theta\sin 2\phi\cos\psi]$	$\sqrt{\frac{5}{8}}[\sin 2\theta(-\cos\theta\sin 2\phi\sin\psi + \cos 2\phi\cos\psi) + \sin^3\theta\sin 2\phi\sin\psi]$
$\|\delta c>$	$\frac{\sqrt{15}}{2}\cos\theta\sin^2\theta\cos 2\phi$	$\sqrt{\frac{5}{8}}[\sin 2\theta(\cos\theta\cos 2\phi\cos\psi - \sin 2\phi\sin\psi) - \sin^3\theta\cos 2\phi\cos\psi]$	$\sqrt{\frac{5}{8}}[\sin 2\theta(-\cos\theta\cos 2\phi\sin\psi - \sin 2\phi\cos\psi) + \sin^3\theta\cos 2\phi\sin\psi]$
$\|\psi s>$	$\sqrt{\frac{5}{8}}\sin^3\theta\sin 3\phi$	$\frac{\sqrt{15}}{4}\sin^2\theta[\cos\theta\sin 3\phi\cos\psi + \cos 3\phi\sin\psi]$	$\frac{\sqrt{15}}{4}\sin^2\theta[-\cos\theta\sin 3\phi\sin\psi + \cos 3\phi\cos\psi]$
$\|\psi c>$	$\sqrt{\frac{5}{8}}\sin^3\theta\cos 3\phi$	$\frac{\sqrt{15}}{4}\sin^2\theta[\cos\theta\cos 3\phi\cos\psi - \sin 3\phi\sin\psi]$	$\frac{\sqrt{15}}{4}\sin^2\theta[-\cos\theta\cos 3\phi\sin\psi - \sin 3\phi\cos\psi]$

in C_3 symmetry can be expressed as[18]

$$H_{CF} = B_{20}C_{20} + B_{40}C_{40} + B_{60}C_{60} + \mathrm{Re}(B_{43})(C_{4-3} - C_{43}) + \boldsymbol{i}\,\mathrm{Im}(B_{43})(C_{4-3} + C_{43}) + \mathrm{Re}(B_{63})(C_{6-3} - C_{63}) + \boldsymbol{i}\,\mathrm{Im}(B_{63})(C_{6-3} + C_{63}) + \mathrm{Re}(B_{66})(C_{6-6} + C_{66}) + \boldsymbol{i}\,\mathrm{Im}(B_{66})(C_{6-6} - C_{66}) \quad (1)$$

where Re(x) and Im(x) denote the real and imaginary parts of the complex number x. The number of nonzero crystal field coefficients, B_{kq}, is determined by symmetry. As discussed below, the coordinate system can be chosen to make Im(B_{43}) vanish, so that for C_3 symmetry there are six nonzero values: B_{20}, B_{40}, B_{43}, B_{60}, B_{63}, and B_{66}. Two of the values (B_{63} and B_{66}) can have both real and imaginary parts, making a total of eight crystal field parameters.

The Angular Overlap Model (AOM) Ligand Field. In the most general ligand field there are 27 nonzero real and imaginary parts of the crystal field parameters B_{kq} ($k = 2, 4, 6$; $q = 0,\ldots, k$), and these can be related to the 27 independent matrix elements of the ligand field in the real f-orbital basis $\langle u|V|v\rangle$. This number of independent parameters is equal to the number of upper diagonal elements in a 7×7 matrix minus 1 because the trace of the matrix (the spherical term B_{00}) is absorbed into E_{av}. Urland[19] has provided the relationships between B_{kq} and $\langle u|V|v\rangle$, and this is given in Table 3 of ref 19. However, we require a way to specify the π bonding in the $\langle u|V|v\rangle$ matrix. The $F^{(f)}$ matrix given in Table 2 of Urland[19] is only for axially symmetrical ligands. For anisotropic ligands, where $e_{\pi x} \neq e_{\pi y}$, we must have a way of specifying the x_L and y_L axes of the ligand. This is usually done by including the third Euler angle ψ into the rotational transformation matrix between ligand and metal axes.[20] When these are then substituted as the directional cosines in Table 1 of Urland,[19] after some algebraic manipulation, one obtains the $F^{(f)}$ matrix with x_L and y_L ligand axes defined in terms of ψ. We give a portion of this matrix in Table 2 for σ, π_x, and π_y bonding only. The angles in this table are the usual AOM angles, θ_j, ϕ_j, and ψ_j, which can be defined as follows.[20] We take the metal-centered x_M, y_M, and z_M axes that are initially coincident with a fixed X, Y, and Z molecular axis system and rotate them onto the x_L, y_L, and z_L axis system of the jth ligand. First, the x_M, y_M, and z_M axes are rotated about the Y axis away from Z by the angle θ_j. The x_M, y_M, and z_M axes are then rotated about the Z axis by φ_j to make z_M and z_L collinear. Finally, x_M and y_M are rotated about z_M by ψ_j to align x_M and y_M with x_L and y_L.

Discussion

The fitting of the ligand-field energy levels in Er(trensal) presents a challenge due to the low C_3 point group symmetry and the limited data available in the optical window below 25 000 cm^{-1}. This means both that many parameters are required to describe the ligand field and that some compromises have to be made in the specification of the atomic parameters. However, it was possible to obtain an excellent description of the energies and wave functions of the ground-state multiplet and a fair agreement with the excited-state levels, where most of the experimental features are reproduced. We outline our approach below.

The Structure of the Complex. Referring to Figure 1, we define a molecular coordinate system with the Z axis collinear with the C_3 axis, the Y axis perpendicular to the N1−Er−N2 plane, and the X axis completing a right-handed coordinate system. The *positions* of the seven coordinating atoms can then be defined by the three independent bond lengths (Er−N1, Er−N2, Er−O) and the three angles θ_{N2}, θ_O, and φ_O. θ_{N2} and θ_O are the angles by which the atoms N2 and O, respectively, are rotated away from the Z axis. ϕ_O is the angle by which the O atom must be rotated about the Z axis to be moved into the XZ plane. A π-bonding anisotropy of N2 and O is expected with respect to the aromatic plane. The further two angles ψ_{N2} and ψ_O describe the orientations of these planes. The five angles θ_{N2}, θ_O, ϕ_O, ψ_{N2}, and ψ_O necessary for an AOM description of the geometry[18] are given in Table 3.

Rationalizing the Ligand Field in Terms of the AOM Model. In principle, the crystal field parameters, B_{kq}, can be expressed as a function of the angular coordinates θ_j, ϕ_j, and ψ_j of the ligands and the bonding parameters $e_t(j)$ ($t = \sigma, \pi_x, \pi_y$) using the methods of Urland.[19] In what follows, we have used $\sigma(j)$, $\pi_x(j)$, and $\pi_y(j)$ to denote $e_\sigma(j)$, $e_{\pi x}(j)$, and $e_{\pi y}(j)$, respectively. By the use of the explicit fixed geometry of Er(trensal) from the structural data (Table 3) the $\sigma(j)$ and $\pi_y(j)$ parameters are allowed to vary to see if the B_{kq} values that were obtained from fitting the experimental energy levels could be reproduced.

(18) Goerller-Walrand, C.; Binnemans, K. In *Handbook on the Physics and Chemistry of Rare Earths*; Gschneidner, K. A., Eyring, L., Eds.; North-Holland: Amsterdam, 1996; Vol. 23, pp 121−283.
(19) Urland, W. *Chem. Phys.* **1976**, *14*, 393.
(20) Schäffer, C. E. *Struct. Bonding (Berlin)* **1968**, *5*, 68.

Table 3. The AOM Structural and Bonding Parameters for Er(trensal)

ligand		AOM angles[b]			AOM params		
	i	θ_i	ϕ_i	ψ_i	$e_\sigma(i)$	$e_{\pi x}(i)$	$e_{\pi y}(i)$
N1	1	0	0	0	σ(N1)	0	0
N2	2	θ_{N2}	ϕ^a	ψ_{N2}	σ(N2)	0	π_y(N2)
N2′	3	θ_{N2}	$\phi + 120°$	ψ_{N2}	σ(N2)	0	π_y(N2)
N2″	4	θ_{N2}	$\phi + 240°$	ψ_{N2}	σ(N2)	0	π_y(N2)
O	5	θ_O	$\phi + \phi_O$	ψ_O	σ(O)	0	π_y(O)
O′	6	θ_O	$\phi + \phi_O + 120°$	ψ_O	σ(O)	0	π_y(O)
O″	7	θ_O	$\phi + \phi_O + 240°$	ψ_O	σ(O)	0	π_y(O)

[a] ϕ determines the orientation of the x and y axes, see text. [b] $\theta_{N2} = 66.5$, $\theta_O = 122.07$, $\phi_O = 51.64$, $\psi_{N2} = 36.2$, and $\psi_O = 53.9°$.

There are a number of reasons why this may be of interest. First, we wish to see how far the B_{kq} parameters can be rationalized in terms of local metal−ligand bonding. Second, we wish to see if reasonable AOM parameters can lead to B_{kq} values that are useful as rough starting values for a ligand-field fit in general. Third, this approach can also be used to check the consistency of the fitted B_{kq} values with regard to sign ambiguities. In addition, the AOM may prove to have some predictive value in the Ln(trensal) series. This is because the AOM uses the *actual* molecular geometry of the problem rather than just its molecular symmetry. In the present case we require only five AOM parameters to reasonably describe the problem (three σ-bonding parameters for the three independent bonding atoms and two π-bonding parameters for N2 and O atoms), whereas the crystal field approach requires the eight parameters: B_{20}, B_{40}, Re(B_{43}), B_{60}, Re(B_{63}), Im(B_{63}), Re(B_{66}), and Im(B_{66}).

However, the inherent advantage of the AOM in treating a low symmetry *but known* geometry with a smaller number of parameters introduces additional problems if the axes are not determined by symmetry. In Er(trensal) the Z axis is defined as collinear with the 3-fold axis, but the positions of the X and Y axes are arbitrary within the plane perpendicular to this. The choice of how the X and Y axes are defined changes the phase of the $B_{kq}(q\neq0)$ values, so that a general choice will introduce a nonzero Im(B_{43}). We define an additional angle ϕ that the X axis makes with the N2−Er−N1 plane. There exists a value of ϕ (($\phi + 120°$) and ($\phi + 240°$)) in which Im(B_{43}) = 0. We stress again that in the C_3 point group this value is not determined by symmetry. If the molecular geometry was such that $\phi_O = -60°$ and there were no π-bonding anisotropy, then the molecule would have C_{3v} symmetry and the X axis would be confined to the mirror plane by symmetry ($\phi = 0$). This results in all B_{kq} being real. However, for the actual C_3 geometry in the present case, ϕ will be a complicated function of both the geometry *and* the bonding parameters. It is important to specify this angle, ϕ, otherwise the crystal field and AOM calculations are effectively using different coordinate systems and the parameters cannot be directly compared. Not only will Im(B_{43}) be nonzero but the phase of *all* $B_{kq}(q\neq0)$ will also change.

In the absence of π bonding, the angle ϕ is given by the explicit formula

$$\tan 3\phi = \frac{-\sigma(\mathrm{O}) \sin 3\phi_O \sin^3 \theta_O \cos \theta_O}{\sigma(\mathrm{O}) \cos 3\phi_O \sin^3 \theta_O \cos \theta_O + \sigma(\mathrm{N2}) \sin^3 \theta_N \cos \theta_N} \quad (2)$$

For the geometry of Er(trensal) given in Table 3 and setting σ(N2) = σ(O), one finds $\phi = 4.3°$. Note that eq 2 above does not contain contributions from axial ligands, so it is also applicable to six-, seven-, or eight-coordinate C_3 complexes with 0, 1, and 2 axial ligands, respectively, as long as the ligands have their π-bonding parameters equal to zero. The equivalent expression for π(N2) and π(O) ≠ 0 is much more complex, and in practice, we numerically calculate the value of ϕ that satisfies Im(B_{43}) = 0. In this way, we can directly compare the B_{kq} from different calculations.

Table 4. The Parameters of the Ligand-Field Hamiltonian for Er(trensal)

param[a]	value (cm^{-1})	param	value (cm^{-1})
E_{av}	35 662	B_{20}	−720
F^2	98 935	B_{40}	−44
F^4	70 940	B_{43}	−2121[c]
F^6	49 585	B_{60}	988
a	17.5	B_{63}	353 − *i* 92
ζ_{so}	2371	B_{66}	545 − *i* 311
N[b]	52	σ[d]	20

[a] Other minor atomic parameters are taken from ref 10. [b] Number of assigned energy levels included in the fit. [c] The X and Y axes can always be chosen to make B_{43} real, see text. [d] Root-mean-squared deviation between calculated and observed energies.

Table 5. The AOM Parameters Fitted to the Crystal Field Parameters

params	calcd A[a] (cm^{-1})		calcd B[b] (cm^{-1})
σ(N1)	369		405
σ(N2)	686		624
σ(O)	264		316
π_y(N2)	631		608
π_y(O)	402		419
ϕ (°)	1.77		1.10
	fitted values[c] (cm^{-1})[c]	calc (cm^{-1})	calc (cm^{-1})
B_{20}	−720	−596	
B_{40}	−44	−182	−171
B_{43}	−2121	−1921	−1894
B_{60}	988	1036	1076
B_{63}	353 − *i* 92	758 − *i* 28	702 + *i* 58
B_{66}	545 − *i* 311	326 − *i* 571	347 − *i* 545

[a] All B_{kq} values are included in the fit. [b] B_{20} is not included. [c] See Table 4.

The required expressions for the eight B_{kq} in Table 4 and for Im(B_{43}) in terms of the AOM parameters were derived using Mathematica. The resulting long and complicated expressions will not be repeated here but can be used to calculate B_{kq} numerically. We investigated a forced "fitting" of the σ(N1), σ(N2), σ(O), π_y(N2), and π_y(O) parameters to the B_{kq} values found experimentally and then recalculated the B_{kq} values from the "fitted" AOM parameters. It is of interest to know (i) if the resulting AOM parameters have chemical significance and (ii) if the B_{kq} parameters can be successfully expressed in a smaller number of AOM parameters. The reduction of the number of parameters may be possible because independent information about the *actual* geometry of the molecule is used rather than just the symmetry.

Table 5 contains the AOM parameters fitted to the experimental B_{kq} values, given in Table 4, as well as the "recalculated" B_{kq} values. Several comments can be made. The σ AOM parameters are smaller by an order of magnitude than those typically found for transition metal complexes.[21,22] This is not surprising due to the shielded nature of the f electrons. However, the π parameters are of the same order as the σ parameters. Of the resulting recalculated B_{kq} parameters shown in Table 5,

(21) Gerloch, M.; Slade, R. C. *Ligand-Field Parameters*; Cambridge University Press: Cambridge, 1973.
(22) Lever, A. B. P. *Inorganic Electronic Spectroscopy*, 2nd ed.; Elsevier: Amsterdam, 1984.

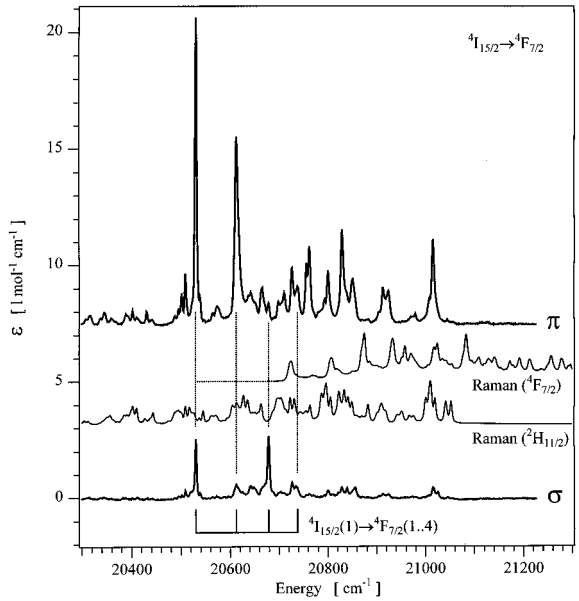

Figure 4. Detail of the $^4I_{15/2} \rightarrow {}^4F_{3/2}$ absorption spectrum measured at 10 K in σ (upper) and π (lower) polarization. The experimentally assigned ligand-field levels of the $^4F_{3/2}$ states are shown (bottom). The two central curves are Raman spectra that have been convoluted with the electronic origins of the $^4F_{3/2}$ multiplet (upper) as well as the lower energy neighboring $^2H_{11/2}$ multiplet (lower).

reasonable agreement was found for the signs and magnitudes except for Im(B_{63}). The agreement with B_{20} is probably fortuitous, as it is well-known[17] that this parameter depends on long-range interactions. The last column of Table 5 contains the AOM and the recalculated B_{kq} parameters without including B_{20}. It is noted that the AOM parameters are quite sensitive to particular B_{kq} values. For example, if B_{40} is small it forces σ(N1) to also become small or even negative, because it depends mainly on the $\langle z^3|V|z^3\rangle$ matrix element.[19]

There is the question of whether the relatively large AOM π-bonding parameters represent actual π bonding or whether they are artifacts of the fitting process. Previous studies on the role of π bonding in lanthanide complexes have seen similar trends to that observed here.[23,24] In a study of Cs_2NaMCl_6 epasolites, a consistent fit of AOM parameters was obtained for a series of six lanthanides. The e_σ/e_π ratio was found to be $\sim$2.5, which is about half the ratio typically found for transition metal chlorides.[22] The even smaller ratio found here may be due to the larger π bonding from the aromatic nature of the ligand.

Vibronic Activity. In some multiplet groups, transitions are observed that cannot be assigned to electronic transitions (Figure 4). Comparison with the Er(trensal) Raman spectrum shows a close resemblance of many of the dominant nonelectronic features in the absorption spectra with the Raman active vibrations of the compound. Surprisingly, these vibronic transitions do not necessarily build on the electronic origins of the excited multiplet under investigation but can originate from the electronic origins of the next lower lying multiplet, as is especially evident for the $^4I_{15/2} \rightarrow {}^4F_{7/2}$ transition (Figure 4). Particularly active are the vibrations in the range 1200−1650 cm^{-1} when they coincide with the energy of a higher energy electronic transition. This may correspond to stretching vibrations within the three bidentate rings that couple strongly to the electronic states of the Er(III) ion. This is unusual, but it appears to be a property of this particular ligand, which imparts a very large ligand field as discussed below.

We have also observed similar vibronic activity in other members of the Ln(trensal) series. These features are not due to impurities as the vibronic transitions differ in energy following the different 4f energy levels. It is also noted that in other complexes, with closely related ligands that do not bind in this heptadentate fashion, these vibronic transitions do not occur.[25]

Ligand-Field Strength. A relative measure of the ligand-field strength is given by the parameter $N_v/(4\pi)^{1/2}$.[26]

$$N_v/(4\pi)^{1/2} = \left[\sum_{k=2,4,6} \frac{1}{2k+1}(B_{k0}{}^2 + 2\sum_{q=1}^{k}|B_{kq}|^2)\right]^{1/2} \quad (3)$$

For the Er(trensal) complex, this value is 1122 cm^{-1} and is, to our knowledge, the largest value reported for an Er(III) complex. This is clearly reflected in the large ligand-field splittings that are observed, for example, the 641 cm^{-1} splitting of the $^4I_{15/2}$ ground-state multiplet. The next largest value of $N_v/(4\pi)^{1/2}$ appears to be for the tris(bis(trimethylsilyl)amido)erbium(III) complex at 1027 cm^{-1}.[26] Other values of $N_v/(4\pi)^{1/2}$ in trigonal Er(III) complexes include Er(ODA)$_3{}^{3-}$ (708 cm^{-1}), Er(C_2H_5-$SO_4)_3\cdot 9H_2O$ (480 cm^{-1}), and Er(III):$LaCl_3$ (319 cm^{-1}).[10] Note that the B_{kq} parameters in ref 10 are expressed in terms of the unit tensor operators and must first be converted to be expressed as in eq 1.[18] It is anticipated that for earlier members of the lanthanide series, the ligand-field strength will be even higher, as the larger metal size will experience relatively strong bonds.

Intensity Calculations. The absorption intensities for individual ligand-field transitions are comparable with those observed for Er(III) coordinated with other organic ligands, such as ODA.[10] The parity forbidden 4f−4f transitions gain their intensity mainly from an admixture of low-lying opposite-parity states, such as the Er(III) 5d states. The onset of the ligand-centered transitions occurs at $\sim$ 25 000 cm^{-1}, as shown in the overview absorption spectrum of Figure 1, and appears to have no significant influence on the 4f−4f transition intensities. When the general intensity parametrization scheme of Reid and Richardson is followed,[27] the present C_3 complex requires 18 intensity parameters for systems with ligands with isotropic polarizability and 27 intensity parameters for systems with anisotropic polarizability. The trigonal Eu(III) complexes of ODA and DBM ligands[28] have previously been shown to require the anisotropic polarizability to simulate the f−f intensities. In this case, the anisotropy was thought to be due to bonds and aromatic rings of atoms not directly bound to the Eu(III) ion.[28] The present system provides an interesting case where the anisotropy is in the bonding of the ligands. However, the Eu(III) complexes were a particularly favorable system to study,[28] in that the ground state was relatively pure and a small subset of intensity parameters could be used. The ground state in the present case is quite mixed, and after many trial calculations, we found that the best agreement with experimental results was obtained when the ground-state multiplet was weighted more in the fit to force a more accurate ground-state wave function. The quality of the fit can be seen in the agreement in the calculated and observed energies for the $^4I_{15/2}$ ground-state multiplet (Table 1) and the intensity calculation of the $^4I_{15/2} \leftarrow {}^4S_{3/2}$ luminescence spectrum shown in Figure 7. This simulation only required the use of isotropic parameters.

(23) Linares, C.; Louat, A.; Blanchard, M. *Chem. Phys.* **1982**, *68*, 453.
(24) Urland, W. *Chem. Phys. Lett.* **1981**, *83*, 116.
(25) Flanagan, M. B.; Bernhardt, P. V.; Lüthi, S. R.; Riley, M. J. Manuscript to be published.
(26) Jank, S.; Amberger, H.-D.; Edelstein, N. M. *Spectrochim. Acta, Part A* **1998**, *54*, 1645.
(27) Reid, M. F.; Richardson, F. S. *J. Chem. Phys.* **1984**, *88*, 3579.
(28) Dallara, J. J.; Reid, M. F.; Richardson, F. S. *J. Chem. Phys.* **1984**, *88*, 3587.

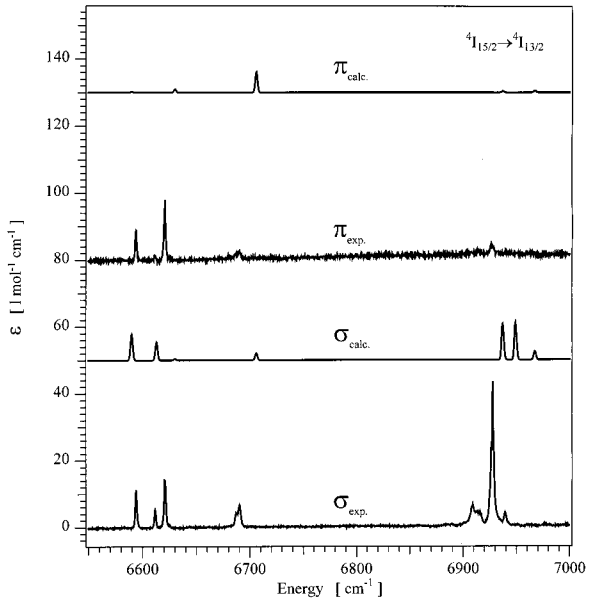

Figure 5. Comparison of the experimental and calculated absorption spectra of the $^4I_{15/2}(1) \rightarrow {}^4I_{13/2}(1...7)$ transitions. The experimental absorption spectra are recorded in σ and π polarization at 10 K with a spectral resolution of 0.48 nm. The simulated spectra are calculated for σ and π polarization in the low-temperature limit. For the calculated energies the parameters from Table 4 were used, and parameters for the intensities are discussed in the text. A Gaussian profile was assumed for all transitions, with a half-width at half-maximum of 1.5 cm^{-1} as typically found in the experimental absorption spectra.

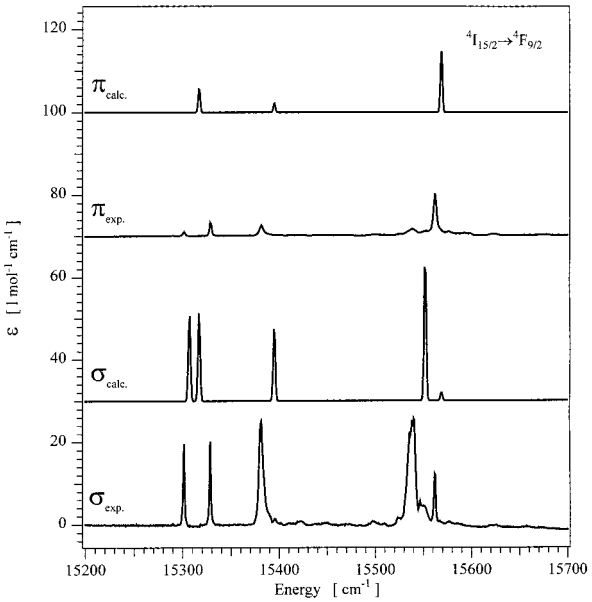

Figure 6. Comparison of the experimental and calculated absorption spectra of the $^4I_{15/2}(1) \rightarrow {}^4F_{9/2}(1...5)$ transitions. The experimental absorption spectra are recorded in σ and π polarization at 10 K with a spectral resolution of 0.1 nm. For the simulated spectrum see caption to Figure 5.

Agreement with the absorption spectrum was fair as shown by the simulation of the $^4I_{15/2} \rightarrow {}^4I_{13/2}$ (Figure 5) and $^4I_{15/2} \rightarrow {}^4F_{9/2}$ (Figure 6) transitions. Other multiplets showed similar agreement except for certain transitions such as $^4I_{15/2} \rightarrow {}^4F_{7/2}(2)$ and $^4F_{5/2}(1)$ where discrepancies of over an order of magnitude were found. Unfortunately, when the anisotropic intensity parameters were included, only very marginal improvements were seen. In this complex, we conclude that it is the accuracy of the wave functions in our relatively primitive ligand-field fit which is the limiting factor and that it is not possible to draw

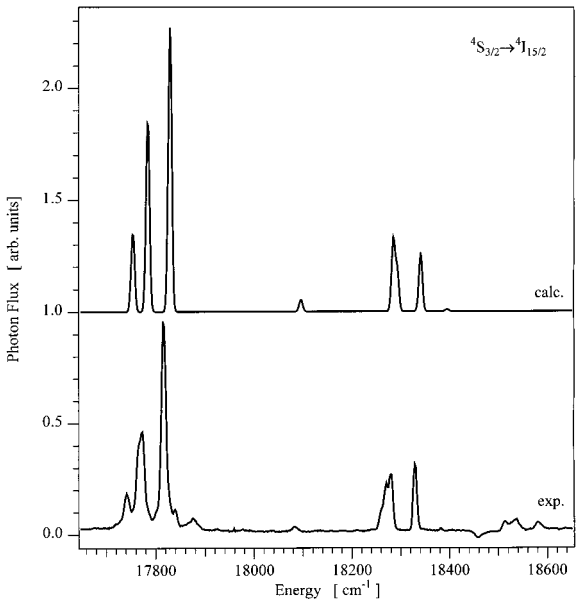

Figure 7. Comparison of the experimental and calculated luminescence spectra of the $^4I_{15/2}(1...8) \leftarrow {}^4S_{3/2}(1)$ transitions. The experimental spectrum was recorded at random polarization at $T = 10$ K with a spectral resolution of 0.2 nm. For the simulated spectrum see caption to Figure 5, except that here the spectrum is calculated for random polarization and a half-width half-maximum of 5 cm^{-1} was used which is comparable to that observed in the luminescence experiments.

conclusions about the necessity of including the π-bonding anisotropy in the calculation of the intensity of the f−f transitions in Er(trensal). It is noted that a recent study[29] has shown that multiple indistinguishable parameter sets can be found in these types of calculations and that the local minima in the fitting process can be numbered in the thousands.

Conclusions

The low-temperature luminescence and polarized absorption spectra of the Er(III) complex of the heptadentate ligand trensal have been measured and the observed f−f transitions have been assigned. The observed energies have been fitted to an electronic Hamiltonian with a ligand-field Hamiltonian of C_3 symmetry. This represents one of the lowest symmetry lanthanide complexes whose f−f spectrum has been reliably assigned and the ligand field has been determined. The sign and magnitude of the crystal field parameters can be broadly rationalized within terms of the AOM, which has proved useful in the analysis of the spectra. It is found that this complex shows a large ligand field, which is the largest yet reported for an Er(III) complex. We plan to further study other complexes in the isomorphous series to determine the applicability in using the AOM in f-electron spectroscopy.

Acknowledgment. Financial support for this research was provided by the Swiss National Science Foundation and the Australian Research Council. We acknowledge M. F. Reid for providing us with his computer program.

Note Added after ASAP. The footnote numbering on p 5402 of this article, incorrect as posted on Sep 6, 2001, is correct as posted on Oct 1, 2001.

Supporting Information Available: Listing of the Mathematica output giving the B_{kq} parameters in terms of the AOM parameters and the angle ϕ. This material is available free of charge via the Internet at http://pubs.acs.org.

IC0103244

(29) Burdick, G. W.; Summerscales, R. L.; Crooks, S. M.; Reid, M. F.; Richardson, F. S. *J. Alloys Compd.* **2000**, *376*, 303−304.